

Probabilistic Seismic Performance Assessment of Tall RC Special Moment-resisting Frame Buildings Equipped with Buckling-restrained Braces under Near-field Excitations

Ali Zarif Moghadam Basefat¹, Hossein Pahlavan^{1*}, Jalil Shafaei¹

¹ Department of Civil Engineering, Faculty of Civil Engineering, Shahrood University of Technology, Shahrood, 36199-95161, Iran

* Corresponding author, e-mail: pahlavan@shahroodut.ac.ir

Received: 29 July 2022, Accepted: 20 October 2023, Published online: 03 January 2024

Abstract

Many tall buildings have already been constructed near faults throughout the world, several of which have sustained casualties and economic losses during strong ground motions. This study investigates the effect of near-fault excitations on the vulnerability of tall, reinforced concrete (RC) special moment-resisting frame (SMRF) buildings equipped with buckling-restrained braces (BRBs) using seismic fragility curves. After attaining the structure's response modification factor (R), three-dimensional (3D) models of 15-, 25- and 35-story frames were developed by the OpenSees software according to the Iranian code provisions. Thus, the seismic response of the elements was obtained. Subsequently, incremental dynamic analysis (IDA) was conducted by selecting a suitable number of compatible accelerograms in two near-field and far-field groups. Considering the maximum story drift as the demand parameter and selecting the interstory drift ratios (IDR) for the slight, moderate, extensive, and complete collapse seismic performance levels proposed by Hazus, IDA curves were plotted. Then, the seismic fragility curves were produced using the structural reliability relations. The median fragility at complete collapse damage level reduced from 0.73 g, 0.62 g, and 0.61 g to 0.68 g, 0.59, and 0.57 g for the 15-, 25, and 35-story near-field and far-field earthquake models, respectively. This was attributed to increasing vulnerability and seismic fragility of the structures as a result of both height increase and distance reduction from fault. Based on the results, the most vulnerable structure, i.e., the 35-story near-fault model, experienced a 40, 17, 18, and 6% increase in median fragility at slight, moderate, extensive, and complete collapse damage levels, respectively.

Keywords

seismic fragility curves, tall buildings, buckling-restrained braces (BRBs), near-fault ground motion

1 Introduction

Investigating the effect of earthquakes on structures as a random and unpredictable phenomenon leads to more accurate results when using probabilistic approaches. These methods can capture different uncertainties in the studied models and in strong ground motions. In this regard, the seismic fragility curve is a convenient tool to estimate structural seismic vulnerability, considering the different uncertainties in earthquakes and structures. Such curves are produced on the basis of the accuracy of the analytic method chosen. For example, in 1981 it was found that the volume of computations will decrease significantly when quantitative uncertainties are replaced with probabilistic parameters and if operators and statistical relations are used instead of mathematical estimations. The obtained relations were then employed in the production

of the fragility curves of a nuclear power plant, which is a sensitive structure and requires accurate evaluations with minimum error and maximum convergence, by taking into account the damage limit states, uncertainties, and peak ground acceleration (PGA) as the probabilistic parameter. Thereon, Kennedy et al. [1] investigated the effect of structural imperfections and different uncertainties on the failure of various critical structural components such as power plants. Several studies have been carried out on the use of seismic fragility curves to assess the risk of earthquakes, evaluate transportation networks, and prepare suitable criteria for seismic performance-based design of structures. Thus, it is critical to establish reliable seismic fragility curves for different types of structures existing in earthquake-prone regions. Besides, fragility curves embrace

different types of uncertainties in capacity or demand, involving various characteristics in material, stiffness, damping, etc. Attention has focused on the significance of loss estimation after the devastating Northridge earthquake in 1994 and later the Great Hanshin (Kobe) earthquake in 1995. However, many have been conducted on the development of structural fragility curves since 2000, mainly for highway bridges.

Engineers have also paid attention to designing earthquake-resistant structures using novel seismic systems that bear higher energy dissipation volumes and stable super-elastic deformations. After the 1966 Parkfield and the 1971 California earthquakes, Bolt used the term "near-fault" for the first time, the importance of which had been neglected in the structural design at the time. Distance from a fault line attracted even more attention after the 1992 Landers, 1994 Northridge, 1995 Kobe, and the 1999 Chi-Chi earthquakes. Distance from fault as a significant source of uncertainty in evaluating the seismic performance of structures has revealed the setback of modern structural systems with acceptable seismic performance and high energy dissipation to counter the initial and destructive pulses of earthquakes at a distance of less than 15 km from the fault, leading the structural and earthquake engineers to build structures with desirable seismic responses [2]. Nonetheless, the difference in near-fault earthquakes with higher destructive indices is completely recognized today. As an undesired shear movement of Earth's crust, an earthquake starts at a point on a fault line and propagates with a velocity as large as the velocity of the shear wave. The propagation of the fault destruction along the site based on the shear wave velocity induces the topmost energy of the earthquake, which is generated by a large pulse, according to Somerville et al. [3], the relationship between dynamic and principal components of the near-fault ground displacements is also complicated. As such, even though the 1994 Northridge and the 1989 Loma Prieta earthquakes did not cause damage to the ground surface, they brought about destructive and intense pulses that are shown as the combination of the principal components in the history of these two strong ground motions. According to Somerville et al. [3], earthquakes with a distance below 15–20 km from the fault line are conventionally considered near-fault. Near-fault ground motions are more destructive than their far-fault companions and are specified with their forward directivity and a large pulse, which is mainly ordinated vertical to the fault line and includes acceleration and velocity pulses. Recently, earthquake-resistant systems with higher energy dissipation

capacity have been considered by researchers to improve the structural behavior against near-fault excitations. Fig. 1 compares the different Northridge earthquake accelerograms in two near-field and far-field stations [3–4].

Implementing braces in building frames is one of the ways to improve the seismic response of the structure. Nevertheless, the connection of such elements in concrete structures is a matter of concern owing to the difference in the nature of the seismic load-resistant system and the building frame in terms of materials and the buckling weakness of conventional eccentric and concentric bracings. Despite the lack of achieving energy dissipation and cumulative ductility considered in conventional types of bracing, buckling-restrained braces with relatively less complicated structure, more straightforward maintenance, higher plasticity, and similar seismic response in tension and compression have received much attention in the seismic design process. The Japanese researchers were the first to investigate buckling-restrained braces (BRBs) in the 1970s. In this respect, Wakabayashi considered the idea of using BRBs by placing flat metal plates between pairs of prefabricated reinforced concrete (RC) panels (Fig. 2). At higher deformations, the brace was more resistant to compression than tension. Later, he developed the idea of embedding a metal core within a metal section with concrete infill [5].

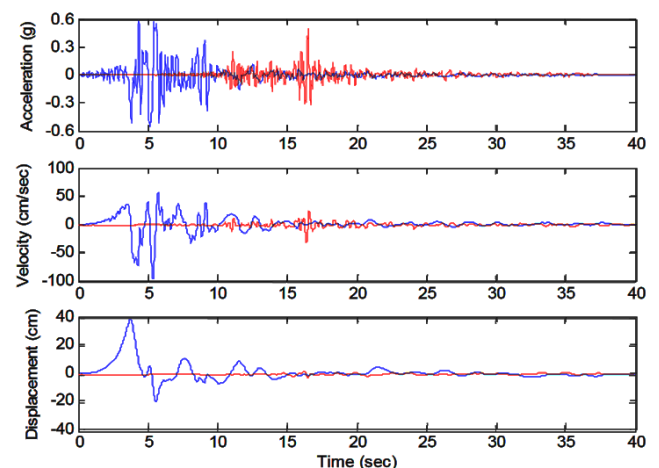


Fig. 1 Comparison of Northridge earthquake accelerograms in two near-field (blue graph) and far-field (red graph) stations



Fig. 2 BRB installation in RC frames

Widespread studies were conducted on this type of bracing, and its implementation gained increase after the Kobe earthquake in Japan (1995). Thereby, the number of buildings constructed with BRBs was around 250 in Japan and 25 in the United States (US) until 2004 [6].

This type of brace was thus recommended in the Journal of Japanese Engineers in 2000 to improve the seismic performance of structures, proceeded by the Structure Journal in 2003. Because of increasing energy absorption and decreasing seismic demand induced by excitations in earthquake-resistant systems, BRBs are also considered in RC frames. These elements are connected to beam-column joints around the span. Concrete structures are exposed to cracking, shrinkage, and drawbacks related to the nonlinear response of the structural system. The types of bracings used in these frames are known as concentric, eccentric, and buckling-restrained braces. Depending on the approach taken, each one of these braces can be used in the structure. Since energy absorption and load-bearing characteristics have been addressed in BRBs, this class of bracing is preferred over other classes. The seismic performance of existing concrete structures is improved by bracing using different approaches such as increasing the life of the structure, changing the use of the building, and reinforcing against natural disasters. Uriz [7] performed experiments on a set of full-scale special concentrically-braced frames (SCBFs) and observed weakness in compression during the buckling of the brace. Such a point of weakness in structures with concentric bracing instigated the main idea of using buckling-restrained braced frames (BRBFs) [7]. Lin et al. [8] compared the reliability of eccentrically-braced frames (EBFs) and BRBFs in compression with that of the moment-resisting frames (MRFs). A series of three-dimensional (3D) nonlinear time-history analysis was carried out for a 5-story building, and the effect of bracing was examined in 5- and 22-story buildings using limit states and interstory drifts recommended by FEMA-356, estimating the probability of failure or that of the limit state. The results revealed that the effect of bracing the frames was increased considerably with increasing ground motions intensity. Braced frames reduced story drifts and failure probabilities against regular ground motions and caused near-fault excitations to input energy into structures over a shorter time span. These characteristics not only avert damage concentration in EBF link beams or BRBF members but also avoid story drift escalation in EBF and BRBF assemblies. Consequently, the supplementary braced frames can relatively resist near-fault earthquakes [8]. Krishnan performed

several case studies on a set of 13-story near-fault moment-resistant frames according to UBC97. He observed that earthquakes measuring 6.7–7.3 on the Richter scale enforce a relative displacement demand of approximately 0.05 and a plastic rotation demand of 4–5% radian in beam-column joints. Thus, it was critical to limit the structural displacements. One of the paramount techniques is the passive control of structures against earthquakes [9]. The effect of structural strengthening on RC frames located near the epicenter of the 2008 Wenchuan earthquake was investigated using simple eccentric braces, BRBs, and viscous dampers. The proper strengthening feature of BRBFs was demonstrated compared to other braces [10]. In 2013, much attention was paid to using BRB as a strengthening element for damaged structures. First, the fragility curve of an RC structure damaged in multiple earthquakes and reinforced with BRB in the second earthquake was obtained [11]. Three concentrically braced frames were designed considering Eurocode provisions to investigate the connection between the brace's behavior and the weak story's occurrence. The results revealed that the designs were inadequate as the global yield mechanism had not been provided, and the buildings were considered to collapse at a lower acceleration level than the design action [12]. In 2014, a full-scale specimen was made in Thailand with an aim to find an energy-based approach to improve non-ductile RC structures. The strengthening method with BRB was advantageous to the overall response of the structure [13]. A study was conducted on different types of BRBs in a damaged RC frame in 2015, and the infill effects were also considered. Full-scale experiments were compared with the literature and had an acceptable accuracy [14]. A research study was conducted on the susceptibility of Eurocode 8 CBF designs to exhibit weak story behavior subjected to seismic action. The focus of the article was on developing supplementary conditions to Eurocode 8 based on plastic analysis. Models of 4-, 6-, 8-, and 10-story-high buildings are built on an orthogonal grid that consists of the same four 6-m bays in both plan directions. Seven artificial accelerograms were selected to respect the minimum requirement of Eurocode 8. So, the average of the results was considered [15]. A study [16] was also conducted on the energy transfer from a BRB to a concrete member in Taiwan. The results showed that the energy could be transferred through a compression block at the connecting point of BRB and the concrete member. A novel performance-based method, based on the notion that BRB undergoes 70% of the story shear, was experimented on a full-scale two-span concrete frame

in 2016 by adding plates at the connection point of BRB to the frame [17]. Hamidi Jamnani et al. [18] investigated the fragility curves of RC structures strengthened by bracing members. They considered an RC intermediate moment-resisting frame designed according to the first version of the Iranian Code and estimated the vulnerability of the structure based on FEMA 356. Three different types of bracing were investigated under 30 earthquake records. Interstory drift and the plastic deformation of bracing were considered the main parameters, where plastic deformation was regarded the most important one among others. The initial state of the structure was considered vulnerable as per Iranian Standard for Seismic Design of Buildings (Code 2800). However, BRBs outperformed both eccentric and concentric braces [18]. The application of BRB had not been addressed in the earlier versions of Eurocode 8 when Zsarnoczay et al. [19] presented a method based on FEMA 695, which only included the design of a 2-story diagonally braced frame with pinned connections and considered BRB capacity against local failures. Many existing RC buildings are constructed based on old seismic standards, and thus, lack structural sufficiency. According to previous studies, BRBs joints can be effective in the seismic improvement of structures. However, Eurocode 8 does not address the design of BRBs. This shortcoming was a significant impediment to using this type of seismic strengthening approach in Europe. Therefore, a numerical method was established and compared as the best approach between two developed variables. Based on this investigation, the parameters that control the design method were calibrated to ensure the collapse threshold performance mentioned in Eurocode 8. Finally, the potential of the proposed design method in achieving performance objectives implicitly considered in the design process was also explored [19]. In 2017, the strengthening of RC structures with lower ductility was proposed as a new method using BRBs. The life-cycle assessment was performed based on the cost of maintenance, where the obtained results were admissible [20]. An educational building with RC frames equipped with BRBs was strengthened based upon Kessay formulation in Portugal in 2019. The results showed a remarkable increase in strength, ductility, and energy dissipation of the RC frames. In this regard, the capacity curve was modified, and the area under the curve was manifolded [21]. Gong et al. [22] showed that BRBs were more effective than other bracing systems in concrete structures. In 2018, a conventional two-story concrete structure equipped with BRB was examined on a real scale in 2018. Given the out-of-plane buckling of

BRBs and the connection plates, the results suggested the design of structures using BRBs [23]. Since the codes focus on drifts when considering nonstructural responses, acceleration-sensitive damages have comparable or greater consequences than drift-sensitive damages. The repair cost calculations were found to be sensitive to nonstructural quantities and the seismic design categorization of their elements. The results suggest that modern building standards do not reliably deliver earthquake resilience. Structural response parameters are used to characterize demands on structural and nonstructural systems determined from nonlinear time history analyses of representative buildings modeled in OpenSees [24]. The performance of concrete structures strengthened with BRBs was evaluated in 2020, considering the demand hazard plots and performing stability analysis. The results revealed the effect of BRB and infill walls on the seismic performance of different components and the impact of strengthening with BRB on a full-scale structure [25]. Pahlavan et al. [26] investigated the fragility curves of RC structures equipped with BRB members. They considered an RC special moment-resisting frame designed according to the fourth version of the Iranian Code and estimated the vulnerability of the structure based on FEMA. A set of reinforced concrete frames (RCFs) and the corresponding BRBs was designed in 2021. The effect of BRB in RCFs with different stories, story shear ratio, and the overall performance of RCFs were investigated. Due to the different responses of BRB and RCFs, their simultaneous function is complicated in the dual structural systems, particularly their seismic responses. Adding BRBs in RCFs changed story shear distribution as well as the axial demand in RC columns and BRBs. In addition, the yield strength, initial elastic stiffness, and energy dissipation of BRB-RCF systems are higher than those of individual frames and braces. Thus, such interaction and synergy should not be ignored in design [27]. Chen and Bai [28] quantified the relationship between stiffness, stability, and the low-cycle fatigue behavior of BRBs. All components' failure indices were evaluated, and seismic performance design indices for the BRB core were optimized, since analytic results can pave the way for developing the design method of BRB-RCF systems. Given that period, story shears, moments, and drifts are considerably high in tall buildings, the vulnerability of these buildings increases when exposed to near-fault earthquakes. Therefore, the application of BRBs in tall RC buildings and the investigation of seismic response of the structure using reliability indices like seismic fragility curves is a less considered issue in the field of

earthquake engineering. This study investigates the effect of distance from a fault on the seismic vulnerability of tall RC buildings incorporating special moment-resisting frames (SMRFs) equipped with BRBs according to HAZUS-MH MR-5 [29] damage levels. After obtaining the response modification factor (R) and desirable structural performance via the energy approach, fragility curves were plotted considering different uncertainties based on the process shown in Fig. 3. According to the seismic evaluation in this project, first, earthquake records were selected in two groups of near-field and far-field motions, and the 3D models of 15-, 25-, and 35-story buildings were analyzed and designed. Next, nonlinear IDA was conducted by OpenSees for the selected records, and nonlinear drift values of stories were achieved. Then, seismic fragility curves were produced for the four damage levels, and the estimations were validated with experimental results and the data in the literature (Figs. 4 and 5, Tables 1–4).

2 Applied methods

2.1 Methodology and numerical models

The lateral load-bearing system used in the 3D modeling of this study was an RC SMRF equipped with BRBs in 15-, 25-, and 35-story buildings. The structural design was performed according to the Iranian National Building Code and the seismic details provided in Code 2800. The characteristics of the models used are as follows:

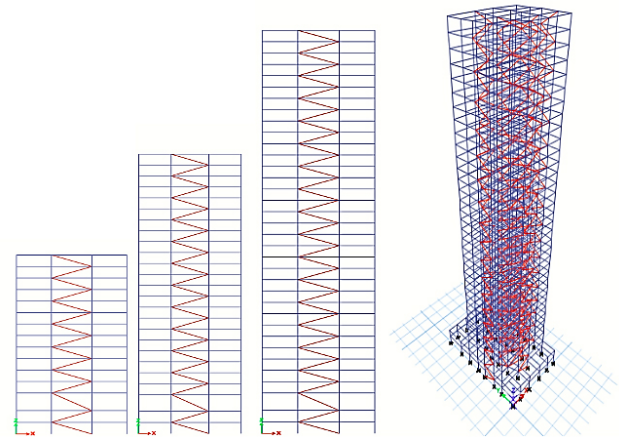


Fig. 4 BRB layout along building height

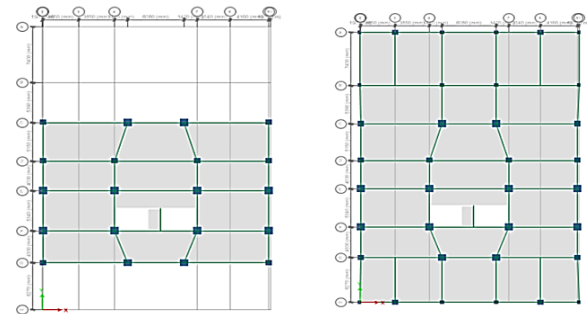


Fig. 5 Plan of stories: (a) parking, (b) other stories

Table 1 Weight, base shear, and overturning moment values of the studied models

Parameter	15-Story Model	25-Story Model	35-Story Model
(Ton) (W)	6367.5	14840.36	16722.87
(Ton) (V)	513.4	756.86	919.76
(M _{OV}) (Ton-m)	7131.53	11885.89	14477.33

Table 2 Beam and column dimensions and rebars of the 15-story model

Stories	Column dimensions (cm)	Column rebar	Beam dimensions (cm)		Beam rebar	
			height × width	Top	Bottom	
1–3	70 × 70	28Φ25	60 × 40	7Φ20	5Φ20	
4–6	60 × 60	20Φ25	50 × 40	7Φ20	5Φ20	
7–9	55 × 55	20Φ25	45 × 40	7Φ20	5Φ20	
10–12	50 × 50	20Φ20	40 × 40	6Φ20	5Φ20	
13–15	40 × 40	16Φ20	40 × 40	6Φ20	5Φ20	

- The structure is located in a region with a very high seismicity risk;
- The site soil is considered Type III;
- The height of the building lobby is 5 m, and the other stories are 3.25 m high;
- The yield stress of the transverse steel in beams and columns is 240 MPa;

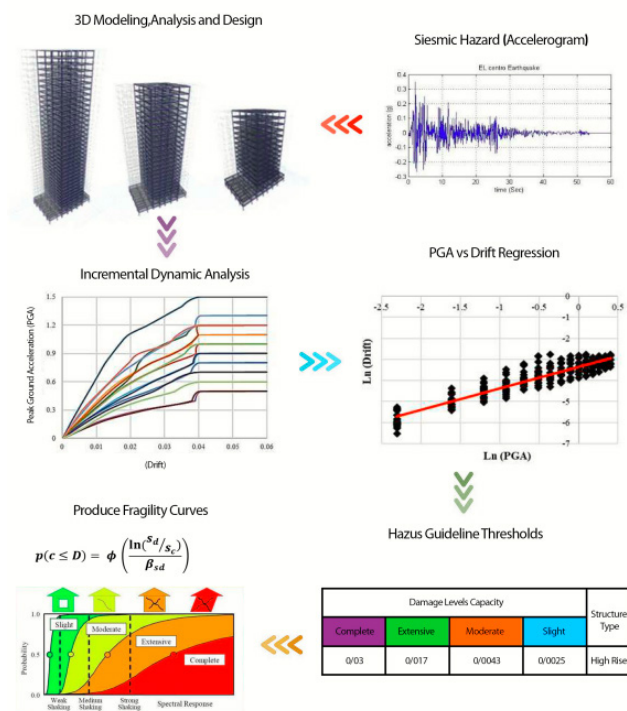


Fig. 3 Implemented Probabilistic seismic assessment procedure

Table 3 Beam and column dimensions and rebars of the 25-story model

Stories	Column dimensions (cm)	Column rebar	Beam dimensions (cm) height × width	Beam rebar	
				Top	Bottom
1–5	95 × 95	40Φ28	95 × 60	8Φ25	7Φ25
6–10	85 × 85	36Φ28	85 × 60	8Φ25	6Φ25
11–15	75 × 75	28Φ28	75 × 50	7Φ25	6Φ25
16–20	65 × 65	28Φ25	65 × 40	7Φ25	5Φ25
21–25	55 × 55	20Φ25	55 × 40	5Φ25	3Φ25

Table 4 Beam and column dimensions and rebars of the 35-story model

Stories	Column dimensions (cm)	Column rebar	Beam dimensions (cm) height × width	Beam rebar	
				Top	Bottom
1–5	120 × 120	48Φ28	100 × 70	9Φ25	8Φ25
6–10	110 × 110	44Φ28	90 × 60	9Φ25	8Φ25
11–15	100 × 100	36Φ28	80 × 60	8Φ25	7Φ25
16–20	90 × 90	28Φ25	70 × 50	8Φ25	7Φ25
21–25	80 × 80	20Φ25	70 × 50	7Φ25	6Φ25
26–30	70 × 70	16Φ25	60 × 40	7Φ25	6Φ25
31–35	60 × 60	16Φ25	60 × 40	5Φ25	3Φ25

- The ultimate stress of longitudinal steel in beams and columns is 370 MPa.
- The concrete grade C30 was used for beams and slabs and C35 for columns. Longitudinal rebars were of AIII type, and stirrups were of AII type. Also, St37 steel was considered for the bracing steel core.

The BRB characteristics were tested at the University of Tehran, Iran, and confirmed by Pooya Tadbir Vira Co. (Vira Brace), an agent for the Robinson Co. The gravity loading conformed to Article 6 of Iranian National Building Requirements (VER 2013) [30]. Moreover, the calculation of the base shear coefficient of the earthquake and the implementation of seismic principles were conducted based on Code 2800 (VER 4) [31].

The considerable weight loss in the studied structures is observed compared with structures with dual systems, specifically heavy shear walls. In this case, high-rise buildings with dual systems approximately weigh 1.4 t/m². Nevertheless, around 30% weight loss was obtained when using BRBs (Table 5).

2.2 Response modification factor

Due to the lack of required information in the seismic design codes, the response modification factor was attained after performing nonlinear static analyses according to the method proposed by Chopra and Chintanapakdee [32]. In the linear design of structures, the earthquake load is obtained from a linear spectrum. The reduction coefficients are then applied to the earthquake load based on factors like ductility, overstrength, degree of indeterminacy, redistribution of loads in the nonlinear zone, damping, etc. The linear force calculated from the linear spectrum is decreased using a reduction coefficient called the response modification factor (R). In the seismic design of structures, buildings remain in the linear region and experience no damage during small earthquakes. They sustain nonstructural damages during moderate earthquakes and incur structural and nonstructural damages in the course of intensive earthquakes. However, the overall stability is maintained, and damage does not exceed a certain level specified by the design code. In this regard, the response modification factor is the linking bridge between the linear and nonlinear responses of the structure. This factor was first referred to by the Applied Technology Council (ATC) in the ATC 3-60 report, and the NEHRP provisions in 1985 based on the ATC reports. A decade later, similar coefficients were suggested by the UBC Code in 1988 to optimize the structural response [33]. Considering that codes remain silent on the characteristics and response of the new lateral load-resisting system, i.e., the RC SMRF equipped with BRB, the bilinear pushover curve

Table 5 The first 5 mode periods of the models and cumulative mass participation percentages

Mode Number	15-story model		25-story model		35-story model	
	Period	cumulative mass participation percentage	Period	cumulative mass participation percentage	Period	cumulative mass participation percentage
First	1.626	67%	2.242	65%	3.746	60%
Second	1.433	69%	2.048	67%	3.52	61%
Third	1.205	70%	1.6	69%	2.508	64%
Fourth	0.631	78%	0.856	79%	1.529	79%
Fifth	0.549	81%	0.752	81%	1.320	80%

(Fig. 6), response modification factor, and the initial ductility ratio were first obtained for the six models using the approach recommended by Priestley and Paulay [35]. Then, the design process was monitored to reach convergence. The area under the idealized bilinear curve was calculated without Microsoft Excel or any other software, only using geometric relations. The linear branch of the idealized pushover curve was continued so that the area under the curve was equal to that of the actual curve. Afterward, the response modification factor, ductility ratio, initial stiffness, and the bearing capacity of the first plastic hinge were conveniently achieved for the ultimate design. In this study, the life safety performance level was considered for the design basis earthquake with a return period of 475 years according to Code 2800 (VER 4). Table 6 reports response modification factors calculated for the RC SMRF frame and BRB. According to this table, $R = 8.5$ was considered for the system comprised of RC SMRF and BRB [34, 35].

$$\frac{\Delta_u}{\Delta_y} = \mu_{max}, \quad \mu = \frac{\Delta_m}{\Delta_y} \quad (1)$$

2.3 Validation of OpenSees model

Two validation methods were used to ensure the modeling process and the accuracy of the obtained results. In addition, the performance results of structures were compared with existing literature in each stage.

First, the first-mode periods of the structures were estimated using OpenSees to validate the modeling and the results. Then, the results were compared with the values provided by the ETBAS software and the empirical relations reported by Code 2800, according to Table 7.

The proximity of periods achieved by OpenSees and the experiments verifies the modeling process in terms of stiffness and mass distribution. Furthermore, modeling

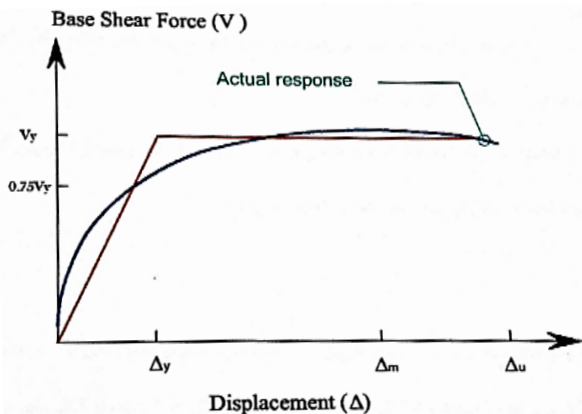


Fig. 6 Priestley and Paulay method [35]

was compared to the experimental test results to validate the materials and elements used. Fig. 7 illustrates the experimental and numerical models of a two-story single-span RC moment-resisting frame subjected to a triangular lateral load pattern with the following specifications:

- The clear span of columns is 350 mm;
- The height of each story is 2000 mm;
- The total height of the frame from foundation to second story is 4600 mm;
- The width and depth of all elements are 300 × 400 mm;
- The longitudinal reinforcements in all beams and columns are laid in two layers (4 rebars at each layer) using $\Phi 20$ rebars. The shear reinforcements and stirrups are $\Phi 10$ rebars at a spacing of 125 mm;
- The compressive strength and elastic modulus of concrete are 30 MPa and 192.5 GPa, respectively;
- The yield and ultimate stress of rebars are 418 and 596 MPa, respectively;
- The concrete compression test was performed on 150 × 300 mm cylinders at the loading rates of 4×10^{-3} and 5.6×10^{-3} for unreinforced and reinforced concrete specimens, respectively. The curing period was 14 days.
- Each column was exposed to a gravity load of 700 kN and a triangular lateral load of 1000 kN in the second story of the experimental model [36].

Table 6 Response modification factors

ASCE-7 (16&22) Response Modification Factor (R)	Calculated R for three models		
	15-story	25-story	35-story
8	10	9.7	9.6

Table 7 Validating of models via periods

Model	Period (s)		
	ETABS	OpenSees	Experimental Method
15-Story	1.62	1.53	15-Story
25-Story	2.24	2.11	25-Story
35-Story	3.75	3.56	35-Story

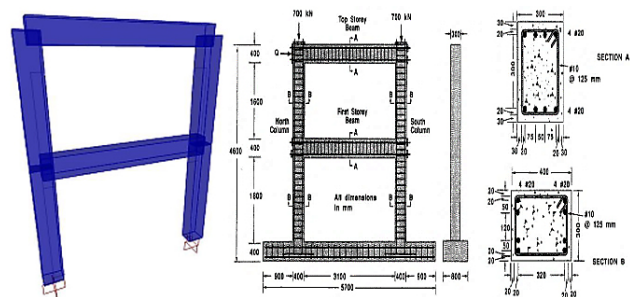


Fig. 7 Reinforcing details of the 2D frame model [36]

The numerical and experimental results, along with the (force-displacement) capacity curves for both models, have been compared in Fig. 7.

2.4 Material and elements

Uniaxial material command was used to define S400 steel rebars, core concrete, and concrete cover. Also, Concrete02 was used to model uniaxial concrete material with tensile strength and linear tensile softening (Fig. 8). Based on Eq. (1), the effect of confinement was modeled by applying the confinement coefficient to the core concrete in the form of an increase in compressive strength of the core concrete compared to the cover concrete, taking into account the confinement coefficient of Mander et al. [37].

$$F'_{cc} = K.F'_{c0}, \quad (2)$$

where F'_{cc} denotes confined concrete compressive strength, and F'_{c0} is the concrete compressive strength.

Likewise, Steel02 was used to define steel rebar based on Giuffre-Menegotto-Pinto (GMP) constitutive model considering isotropic hardening, strength reduction, rupture, and the Bauschinger effect.

Fiber section was also used in defining beam and column cross-sections in OpenSees. Among the characteristics of these fibers, it is possible to apply the characteristics of different materials at any cross-section of the element length. In order to perform nonlinear analyses, element nonlinear Beam Column command was used to define elements considering both the geometric and the material nonlinearity. Coupled with fiber command, this command distributes nonlinear effects throughout elements and directly captures nonlinear cross-section responses at any point using the nonlinear material characteristics. After the nonlinear modeling of materials, cross-sections, and elements, the whole model of the structure was created in OpenSees analogous to the experimental model subjected to gravity and lateral loads. Fig. 9 compares the force-displacement curves obtained from both numerical and experimental models.

Given the good accord of curves in the elastic and plastic regions, the stable superelastic zone up to the strain of 0.002 (Fig. 9), and the excellent conformity of periods between experimental and numerical models (Table 7), modeling can be considered accurate based on the test and empirical relations.

2.5 Selecting accelerograms

According to FEMA P695 [38], the selected accelerograms for the analysis should be suitable to evaluate the

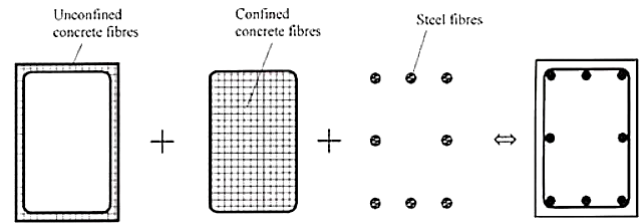


Fig. 8 Fiber division of the RC section [36]

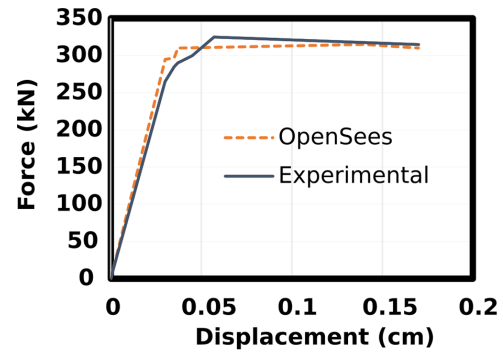


Fig. 9 Comparison of pushover curve in experimental and OpenSees numerical models

probability of vulnerability and structural collapse under the maximum considerable earthquake (MCE). Therefore, these records should meet ASCE 7-16 requirements regarding the three-directional time-history analysis. They should also be strong enough to reflect ground motions as compared to the MCE hazard level. However, the selected accelerograms should be independent of the dynamic and performance features of structures, being applicable for analyzing different structures.

Earthquake record is considered one of the uncertainties in developing seismic fragility curves. According to Shome [39], a total of 10-20 records can accurately estimate the structural vulnerability demand. After scaling accelerograms to 1g, IDA analysis was conducted from 0.1–1.5 g for each model. Table 8 summarizes the properties of 14 accelerograms corresponding to 22 records recommended by FEMA P695 based on distance from the fault, compatibility with site conditions and seismicity of the region, soil type, and fault mechanisms of the selected region.

3 Results

3.1 Seismic response of model members

3.1.1 Cyclic response of frame elements

In the first step, the response and performance of the model under the 1994 Northridge earthquake (N Hollywood-Coldwater Can Station) as a near-field record and the 1971 San Fernando (Gormon-Oso pump Plant Station) as a far-field record were investigated.

Table 8 Selected earthquake records

Record Number	Record Name	Station	Soil Type	Magnitude (R)	Rjb (km)
1	"Duzce_Turkey" 1999	"Duzce"	III	7.14	6.5
2	"ImperialValley06" 1979	"El Centro Array #11"	III	6.53	12.56
3	"Kobe_Japan" 1995	"Takatori"	III	6.9	1.46
4	"Kocaeli-Turkey" 1999	"Yarimca"	III	7.51	1.38
5	"Loma Prieta"1989	"Capitola"	III	6.93	8.65
6	"Northridge"1994	"N-Hollywood -Coldwater Can"	III	6.69	7.89
7	"San Fernando" 1971	"Pacoima Dam (upper left abut) "	III	6.61	0
8	"Duzce_Turkey" 1999	"Yarimca"	III	7.14	97.51
9	"ImperialValley06" 1979	"Coachella" Canal #4	III	6.53	49.1
10	"Kobe Japan." 1995	"Tadoka"	III	6.9	31.69
11	"Kocaeli Turkey"1999	"Mecidiyekoy"	III	7.51	51.17
12	"Loma Prieta"1989	"Bear Valley #12" Williams Ranch	III	6.93	50.71
13	"Northridge" 1994	"Neenach – Sacatara-Ck"	III	6.69	51.61
14	"San Fernando" 1971	"Gormon - Oso Pump Plant"	III	6.61	43.95

The cyclic behavior of elements and the whole structure was examined in OpenSees in the form of moment-curvature hysteresis curves for beam and column elements and force-displacement curves for braces and the entire structure. Hysteresis curves show that beams, columns, and braces have entered the inelastic zone, exhibiting optimal stable superelastic state, and thus, high energy dissipation capacity. Large and stretched hysteresis curves demonstrate no in-cycle strength degradation, increased energy dissipation capacity, and satisfy the nonlinear response considered by the structural model. The similarity between the response of the braces in this study and the actual response of a study performed in 2019 based on the seismic response of BRB elements in a 623-m tall building equipped with outrigger braces consisting of BRB in China also confirms the results of this study [40].

Giving consideration to the results of full-scale experiments on BRBs, cyclic response modeling was carried out in OpenSees in terms of plastic ductility. Then, responses were introduced to the software based on experimental data (6 parameters) as the hysteresis materials. Hence, the curve in Fig. 10 was plotted. The seismic forces imposed from other elements on the studied braces were also investigated.

In like manner, the cyclic response of columns was obtained in terms of the moment around the third axis versus rotation in Fig. 11 in two near-field and far-field states. Stretched and wide curves represent suitable nonlinear seismic responses. Also, the area enclosed by the curves indicates high energy dissipation in the economically-designed structure. Comparing the moment-curvature

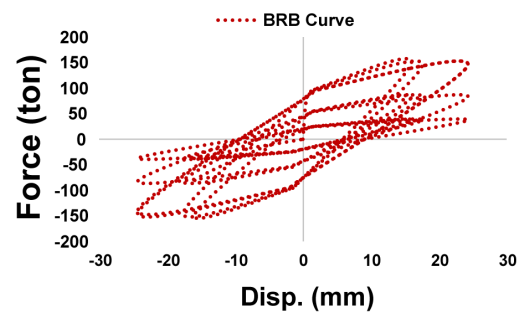


Fig. 10 Hysteresis behavior of BRBs

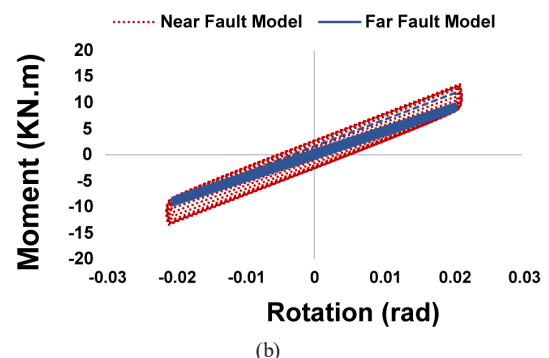
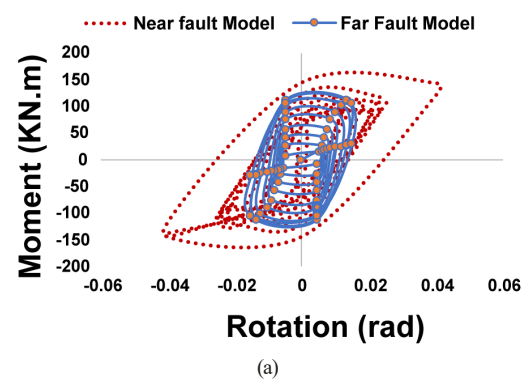


Fig. 11 (a) Hysteresis behavior of RC Columns, (b) Hysteresis behavior of RC Beams

curves between the near-field and far-field structures, it is seen that much more demand is applied to the near-fault structure. In this case, the stable superelastic zone is larger. Nevertheless, on account of the strong primary pulses in the near-fault state, the response shows softening with a greater peak point. The cyclic response of beams based on moment around the third axis versus rotation shows their suitable seismic response and high energy dissipation capacity in an economically-designed structure. The moment-curvature curve in Fig. 11(b) shows much more demand on the near-fault structure and a large stable superelastic zone. The stable nonlinear response in beams is also observed through suitable confinement of braces and high energy dissipation value.

As expected, the cyclic force-displacement curve of the entire structure is shown in Fig. 12. High energy dissipation, no in-cycle degradation in stiffness and strength, and

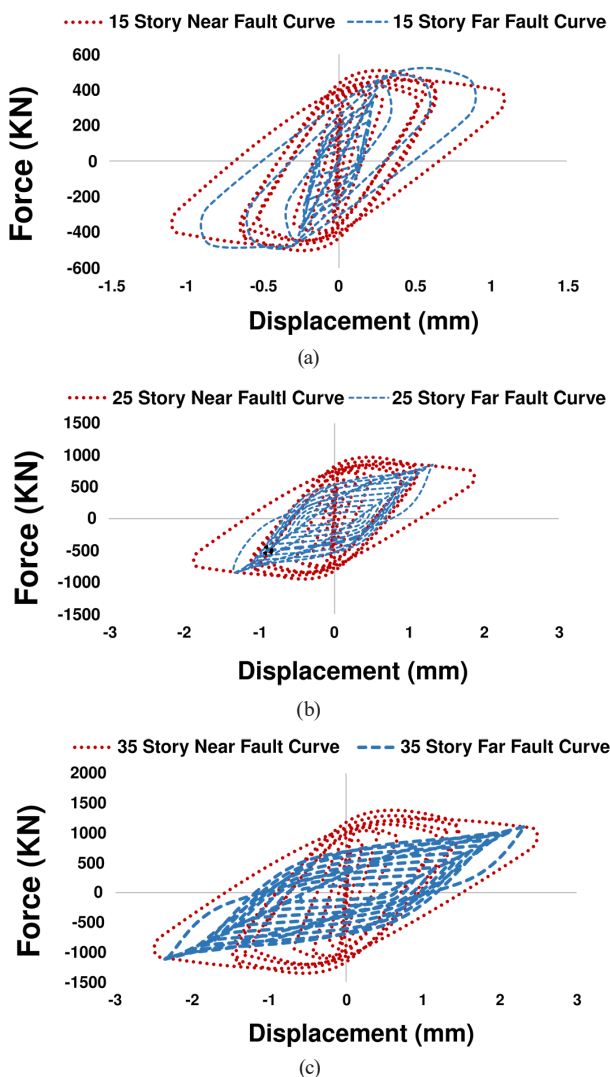


Fig. 12 Near-field and far-field hysteresis curves of models; (a) 15 Story Models, (b) 25 Story Models, (c) 35 Story Models

high ductility is well seen in the diagrams. Considering the destructive primary pulses in the near-fault state, it is possible to compare large initial rotations and residual deformations with those of the common earthquakes in Fig. 12.

3.1.2 Comparison of the base shears and roof displacements for near-fault and far-fault earthquake records

To compare the structural displacements during the earthquake, models were subjected to the near-field 1994 Northridge earthquake (N-Hollywood-Coldwater-Can Station) and the far-field 1971 San Fernando (Gormon-Oso pump Plant Station) records. The residual displacements in these structures, along with cyclic and almost one-sided loading, can be seen in Fig. 13.

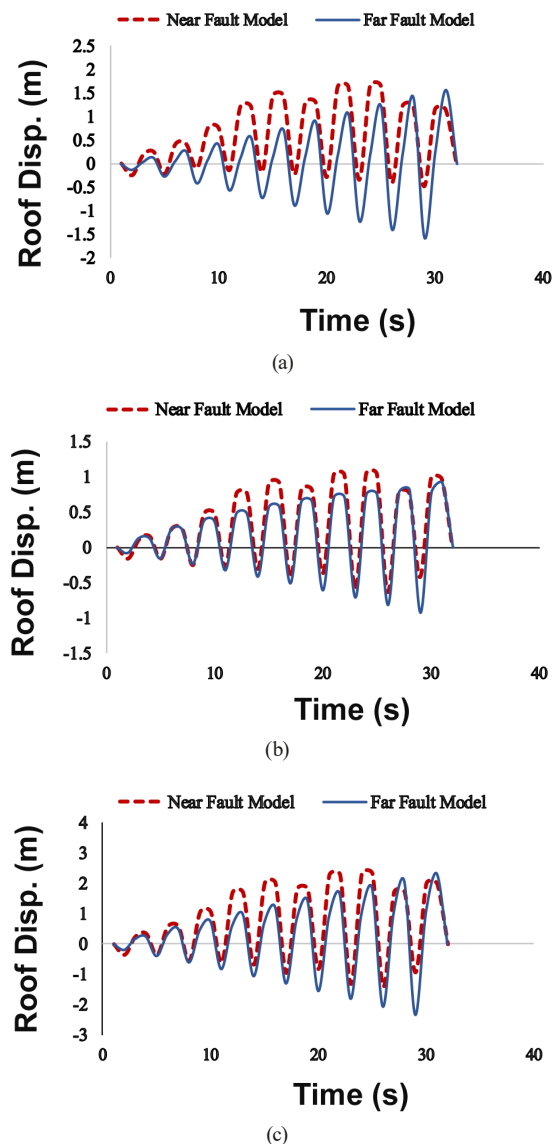


Fig. 13 Near-field and far-field structural responses of models; (a) 15 Story Models, (b) 25 Story Models, (c) 35 Story Models

The capacity curves demonstrate stiffness, strength, ductility, and superelastic zone of the structure. Fig. 14 shows the base shear variations against roof displacement and the effect of distance from a fault on the increase of force-displacement diagrams.

The base shear that a structure near the fault experiences is much higher than the far-field structures, and the stable nonlinear zone is larger. Also, no strength loss after the yield point, together with higher superelastic deformations in near-field structures, confirms the accuracy of the results and assumptions of the current study. Moreover, softening against destructive primary pulses was observed compared to the far-field models.

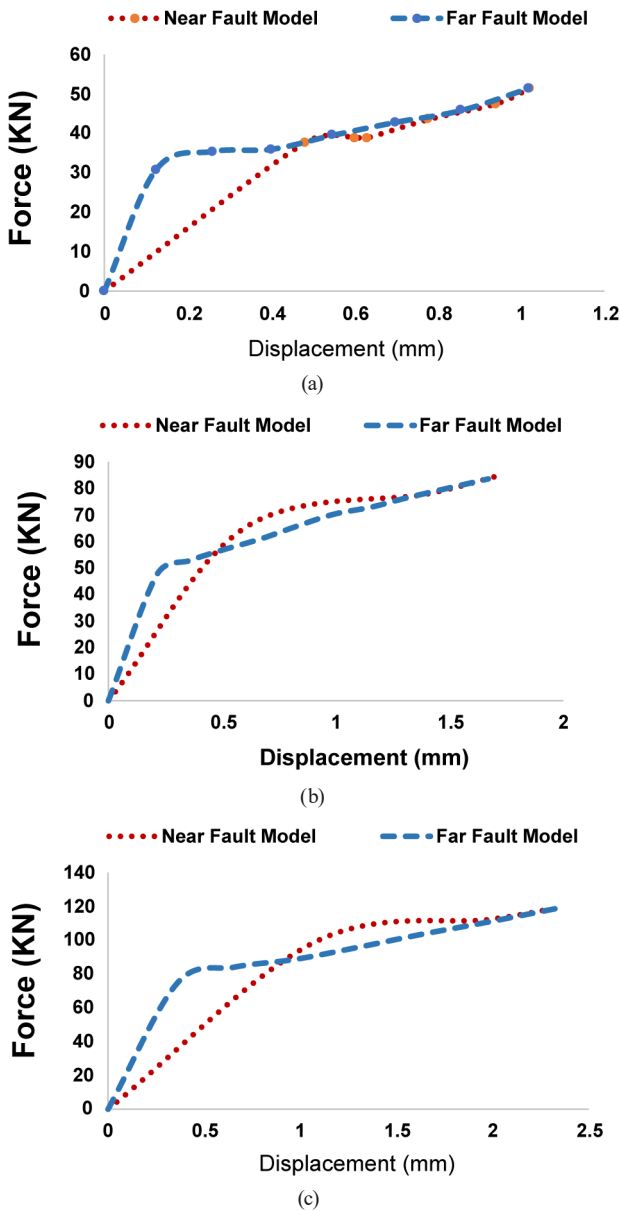


Fig. 14 Near-field and far-field capacity curves of models; (a) 15 Story Models, (b) 25 Story Models, (c) 35 Story Models

3.2 Incremental dynamic Analysis (IDA) results

3.2.1 IDA curves for the models

According to Fig. 15, story drifts are highly influenced by the type of excitation, and the destructive primary pulses affect the third story displacement considerably, where the stiffness is relatively low. For further evaluation, the uncertainty induced by the earthquake is needed. Thus, IDA analyses were conducted for a larger number of records, and subsequent statistical analyses of the results were carried out.

Given the drawbacks of pushover analysis in failing to apply different intensities in time-history analysis, IDA was implemented in this study. IDA is a nonlinear

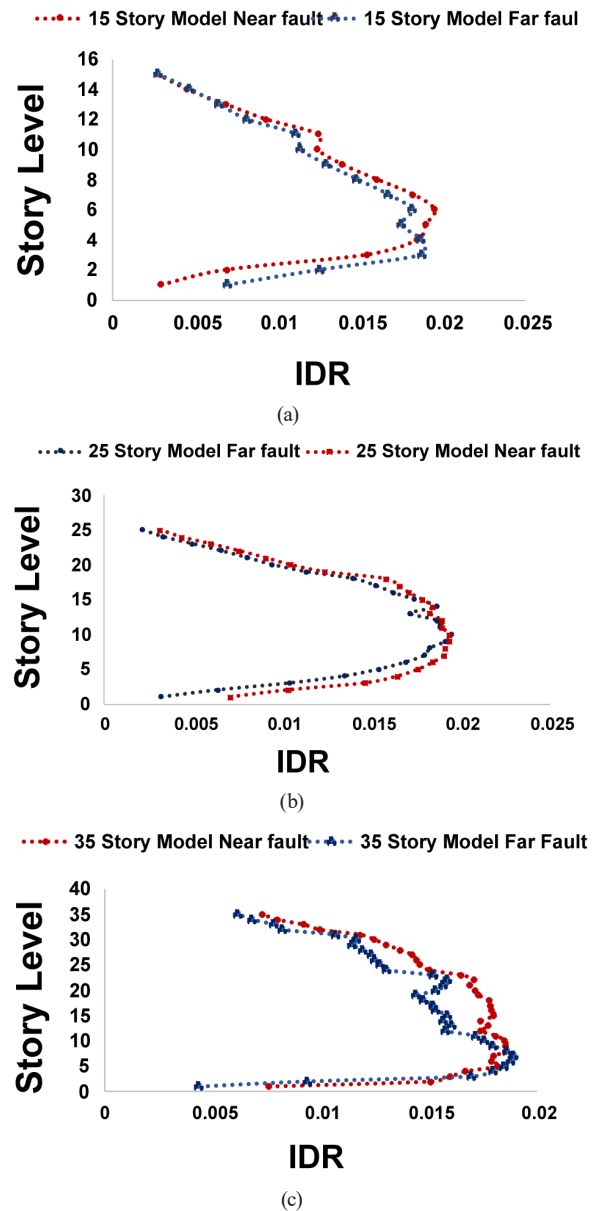


Fig. 15 Near-field and far-field nonlinear drift distributions; (a) 15 story model, (b) 25 story model, (c) 35 story model

dynamic analysis based on the structure's performance, consists of several different steps of nonlinear time-history analysis based on different intensities of peak ground acceleration, and captures structural response in a wide range of different intensities. As shown in hysteresis curves, it is possible to observe the response of structures exposed to earthquakes, from the elastic limit to collapse and overall instability. An elastic area is seen at the beginning of all curves in the form of a straight line, which is almost similar in all IDA curves, after which the nonlinear response appears. Accordingly, it is possible to achieve a general assessment of the building response from complete elasticity to complete collapse by observing IDA curves. As can be seen, the structures enter the nonlinear

region earlier and display lower capacity with the increase in height. It is possible to identify structural capacity, collapse probability, and the percent of exceeding a specific damage limit with the help of IDA. Furthermore, materials with nonlinear behavior can be defined, and dynamic analyses can be conducted using IDA, which are the advantages of IDA over pushover analysis.

In order to analyze the investigated models in this study, PGA was scaled in increments of 0.1 g and imposed on the models until complete failure. The IDA curves were then produced by analyzing the structure at each step. According to Fig. 16, the IDA curves were plotted for 15-, 25-, and 35-story models subjected to near-field and far-field ground motions for the selected 14 accelerograms.

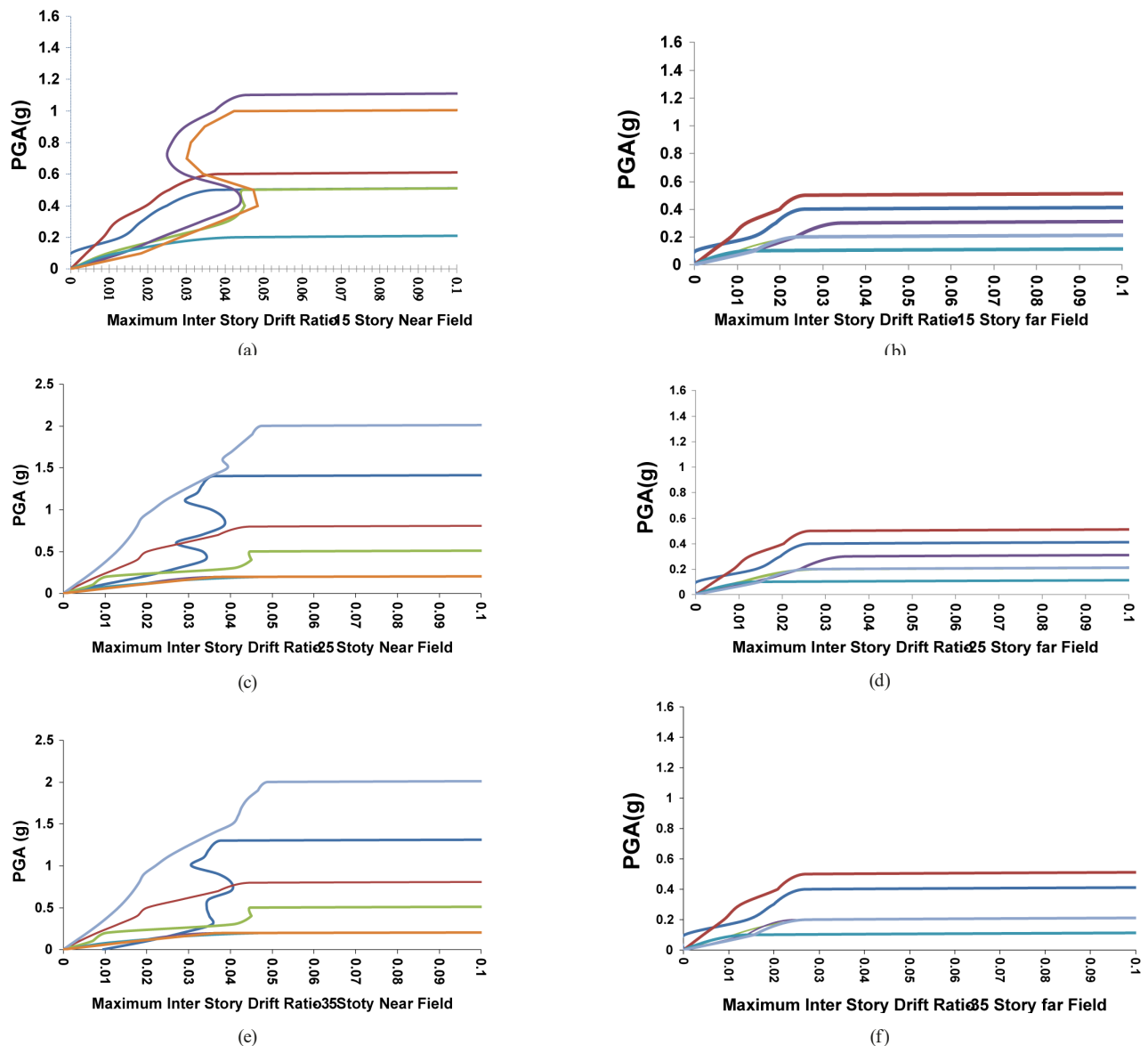


Fig. 16 The IDA curves of models for: (a) near-fault 15-story model, (b) far-fault 15-story model, (c) near-fault 25-story model, (d) far-fault 25-story model, (e) near-fault 35-story model, (f) far-fault 35-story model

As can be seen, the 15-story model has consecutive hardening under near-fault records. Also, softening is observed in near-fault 25- and 35-story models, which stems from the intense displacements induced by the strong primary ground motion pulses.

3.2.2 Defining damage levels

According to HAZUS-MHMR-5, four damage levels were defined in the modeling process. In the slight damage level, the structure remains in the elastic region. In the moderate damage level, minor damage can be conceived. However, major damage is discerned from the onset of extensive level toward the complete collapse damage level. The maximum IDR ratios for the defined damage levels are given in Table 9. According to HAZUS-MH MR-5, softening is observed in the IDA diagrams during the collapse, which is considered the beginning of dynamic instability. The maximum drift thresholds for structural models are listed in Table 9.

3.3 Developing, plotting, and methodology for fragility curves

To develop fragility curves, a probability distribution must be considered for the engineering demand parameters obtained from nonlinear dynamic analysis. Among the most common distributions used in reliability analysis and structural fragility curves are the normal and log-normal distributions. Since no two earthquakes are similar, with a discrepancy in peak acceleration, shaking duration, frequency content, distance from the fault, etc., the earthquake uncertainty should be considered by choosing a sufficient number of suitable records in developing seismic fragility curves. These curves characterize the probability of exceeding a specific damage level concerning the seismicity parameters of the structure. In this study, log-normal distribution was applied to analyze each structure under 14 earthquake records from 0.1–1.5 g of intensity. When structural capacity and seismic demand both follow normal distributions, it is then possible to prove that the consequent composite function will have a log-normal distribution via the central limit theorem. Thus, fragility curves can be written in the form of Eq. (3).

$$P(\leq D) = \Phi \left[\frac{\ln \left(\frac{S_d}{S_c} \right)}{\beta_{sd}} \right], \quad (3)$$

in which x represents PGA, a and b the regression coefficients obtained from the logarithmic regression analysis and interstory drifts against different PGAs, P the exceedance of a certain damage level, D the interstory drift, β_{sd} the standard deviation of the normal logarithm, S_c the allowable limit state, and S_d is the mean of seismic demand. The fragility curves are, in fact, the probabilistic representatives of the structural risk. Fig. 17 shows a logarithmic regression plot, from which coefficients a and b are attained. Based on the explanations in this section, the fragility curves are plotted in the following.

3.4 Seismic fragility curves of models

Figs. 18(a) and (b) shows fragility curves of the 15-story model under near-field and far-field ground motions for the proposed damage levels.

Although slight and moderate damages are not noticeable in structures against near-fault earthquakes, the structure experiences a more fragile state and is likely to collapse given the low drift thresholds in these damage levels. Despite the difference of 40% in slight damage level, the value is within the elastic region, and thus, negligible. Fig. 19 shows fragility curves of the 25-story model under near-field and far-field earthquakes for different damage levels.

As for the 25-story model, performance levels are reached earlier in the near-field earthquake state compared to far-field earthquakes in all damage levels, which is indicative of the effect of building height on increasing fragility. The fragility curves of the 35-story model under near-field and far-field earthquakes for the four damage levels were obtained according to Figs. 20(a) and (b).

Table 9 IDR limit states for high-rise structures HAZUS-MHMR-5

Damage level			IDR
Slight	Moderate	Extensive	Complete
0.0025	0.0066	0.0188	0.05

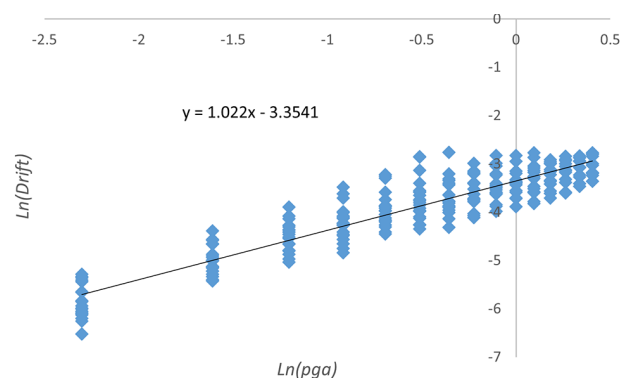
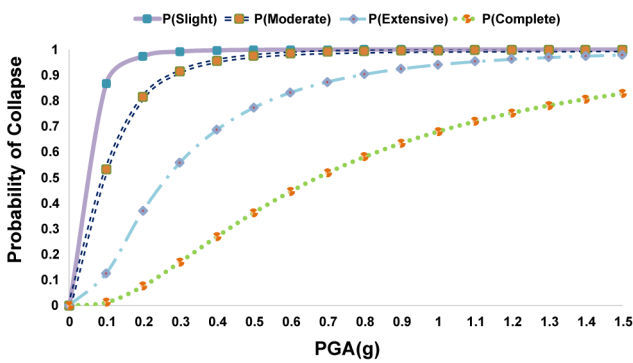
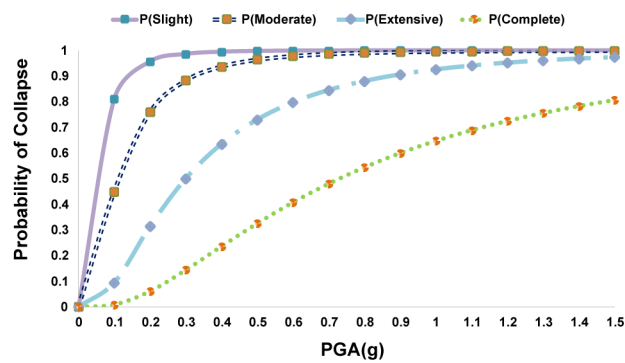


Fig. 17 Logarithmic regression plot

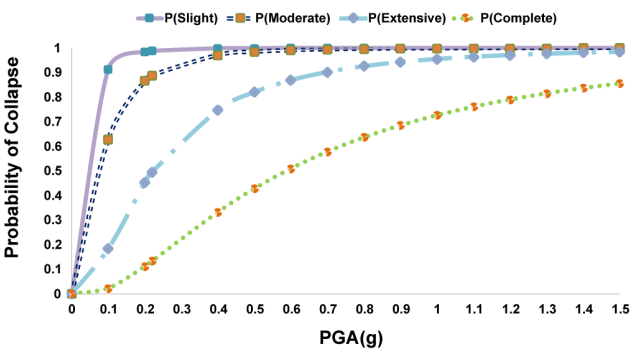


(a)

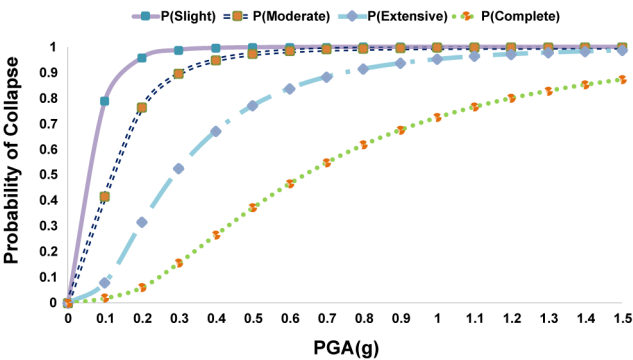


(b)

Fig. 18 Fragility curves of the 15-story model under: (a) near-field, and (b) far-field records



(a)



(b)

Fig. 19 Fragility curves of the 25-story model under: (a) near-field, and (b) far-field records

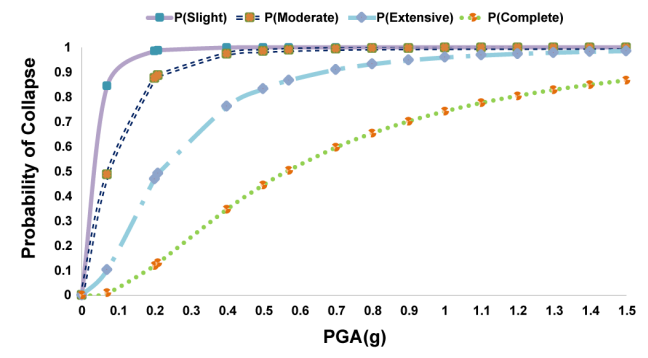
Seismic fragility curves of the 35-story structure show that the structural vulnerability increases in the four damage levels as the distance from the fault is reduced. Comparing Figs. 18, 19, and 20 implies that fragility is increased as the structure height increases. This will be discussed in detail as follows.

4 Conclusions

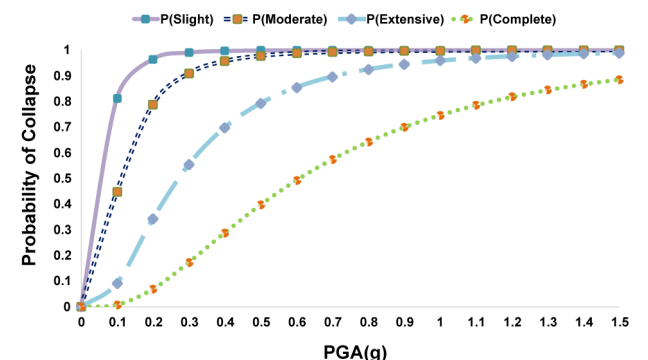
4.1 Comparison of structure fragility curve

4.1.1 Comparison of fragility Curves for the slight damage level

Slight damage level curves are compared with each other for the 15-, 25-, and 35-story structures, as shown in Fig. 21. Based on Fig. 21, the most vulnerable structures are the 35-story and then the 25-story models under near-field records, demonstrating the effect of distance from the fault in slight damage level. The results of the slight damage level fragility curves indicate that the median fragility for the 15-story structure under near-field and far-field records is 0.039 g and 0.049 g, respectively. The corresponding values are 0.031 g and 0.049 g for the 25-story model and 0.03 g and 0.05 g for the 35-story model, respectively. Although the distance from the fault does not



(a)



(b)

Fig. 20 Fragility curves of the 35-story model under: (a) near-field and (b) far-field records

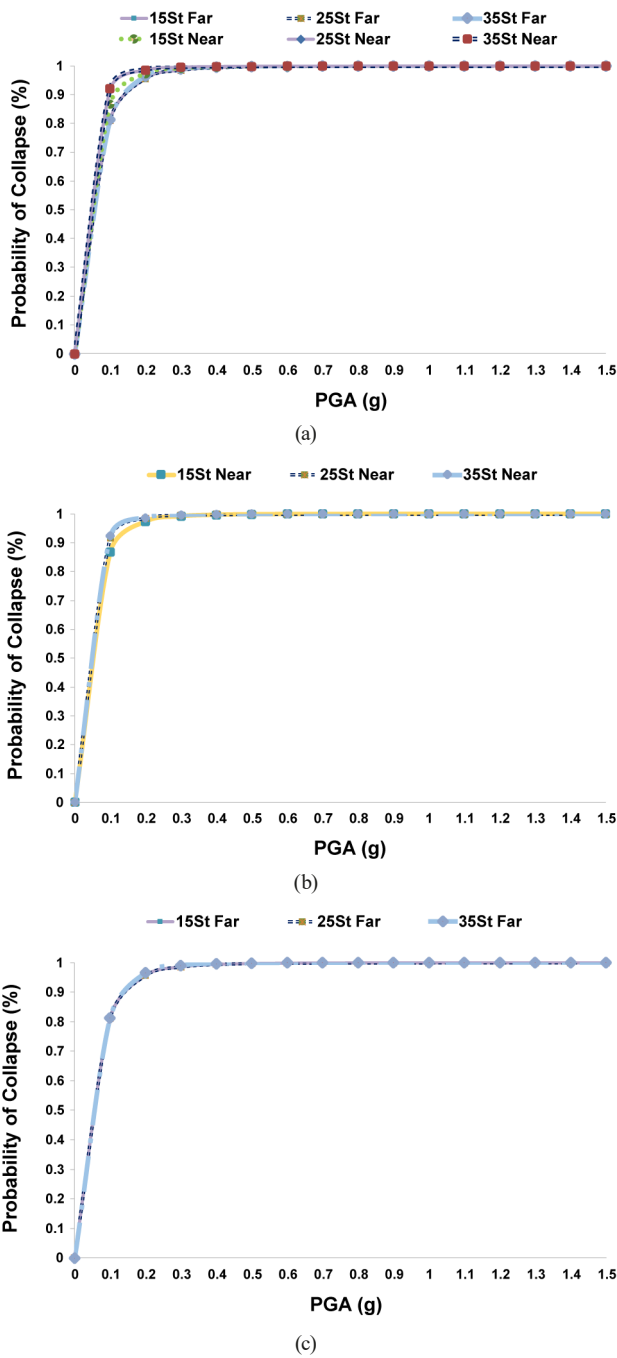


Fig. 21 Comparison of near-field and far-field slight limit state curves; (a) all models, (b) near-field models, (c) far-field models

influence the diagram significantly, a difference of 40% in earthquake acceleration exists in the median fragility to reach this level of damage.

4.1.2 Comparison of fragility curves for the moderate damage level

The most vulnerable structures in the moderate damage level are the 35-story and then the 25-story models under near-fault records, demonstrating the effect of distance

from the fault in the elastic limit state. The median fragility for the 15-story structure in the moderate damage level under near-field and far-field records is 0.093 g and 0.115 g, respectively. The corresponding values are 0.08 g and 0.113 g for the 25-story model and 0.08 g and 0.11 g for the 35-story model, respectively. According to Fig. 22, no significant effect was observed at the level of moderate damage for height increase against distance from the fault. However, comparing slight and moderate damage levels shows the onset of height increase the impact on fragility.

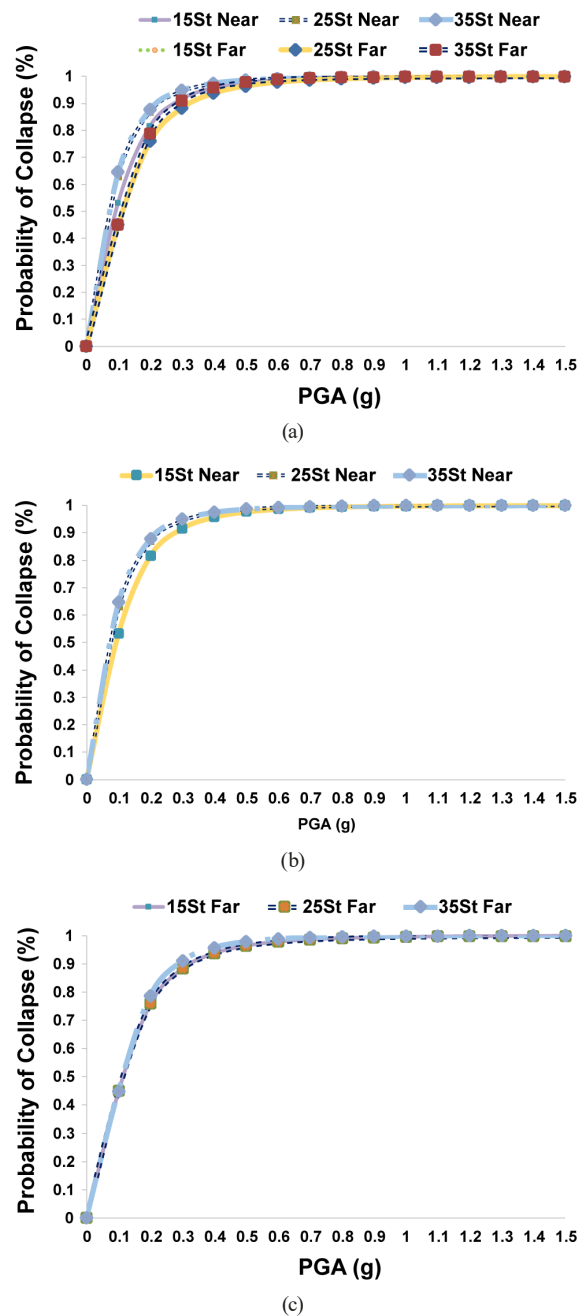


Fig. 22 Comparison of near-field and far-field moderate limit state curves; (a) all models, (b) near-field models, (c) far-field models

4.1.3 Comparison of fragility curves for the extensive damage level

As can be seen in Fig. 23 the most vulnerable structures in the extensive damage level are the 35-story and then the 25-story models under near-fault records. This level is associated with the beginning of damage due to height increase and distance reduction from fault. The median fragility for the 15-story structure in the extensive damage level under near-field and far-field records is 0.027 g and 0.3 g, respectively. The corresponding values are 0.23 g and 0.3 g for the 25-story model and 0.22 g and 0.27 g for the 35-story model, respectively. Although height increase has less effect than distance from the fault, higher buildings are still more vulnerable.

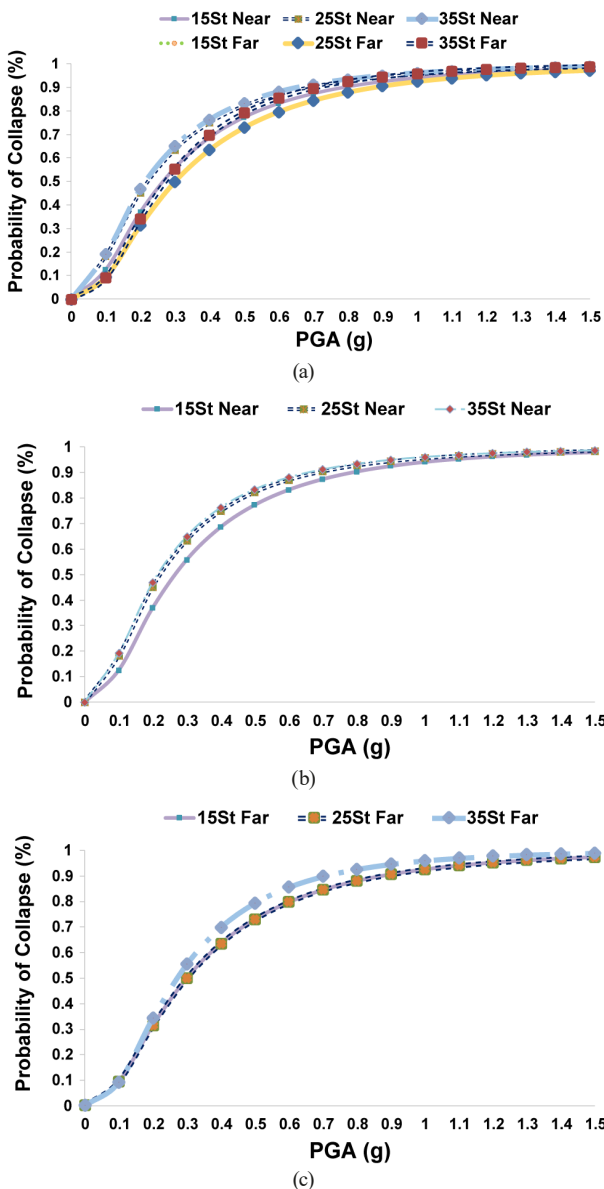


Fig. 23 Comparison of near-field and far-field extensive limit state curves for the three models

4.1.4 Comparison of fragility curves for the complete collapse damage level

According to Fig. 24, the vulnerability of higher and nearer to fault structures is noticeable in the complete collapse damage level, which corresponds to structural instability. The fragility curves results for the complete collapse damage level show that the median fragility for the 15-story structure in the extensive damage level under near-field and far-field records is 0.68 g and 0.73 g, respectively.

The corresponding values are 0.59 g and 0.62 g for the 25-story model and 0.57 g and 0.61 g for the 35-story model, respectively. Fig. 25 illustrates the median fragility of the three models investigated in this research in the form of column diagrams at four levels.

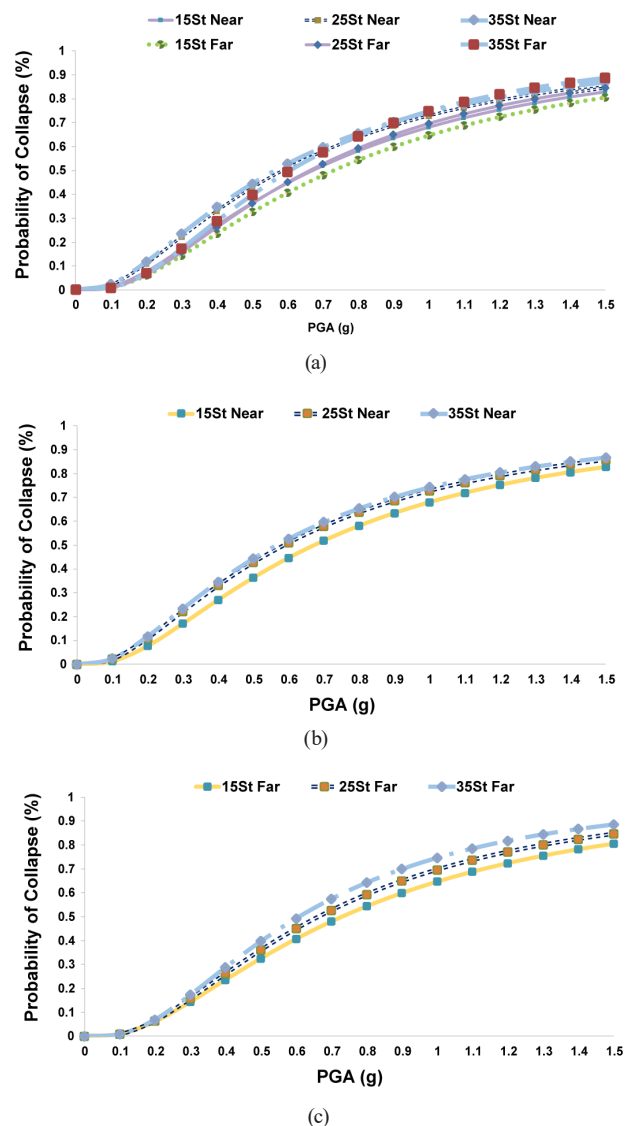


Fig. 24 Comparison of near-field and far-field complete collapse limit state curves for the three models

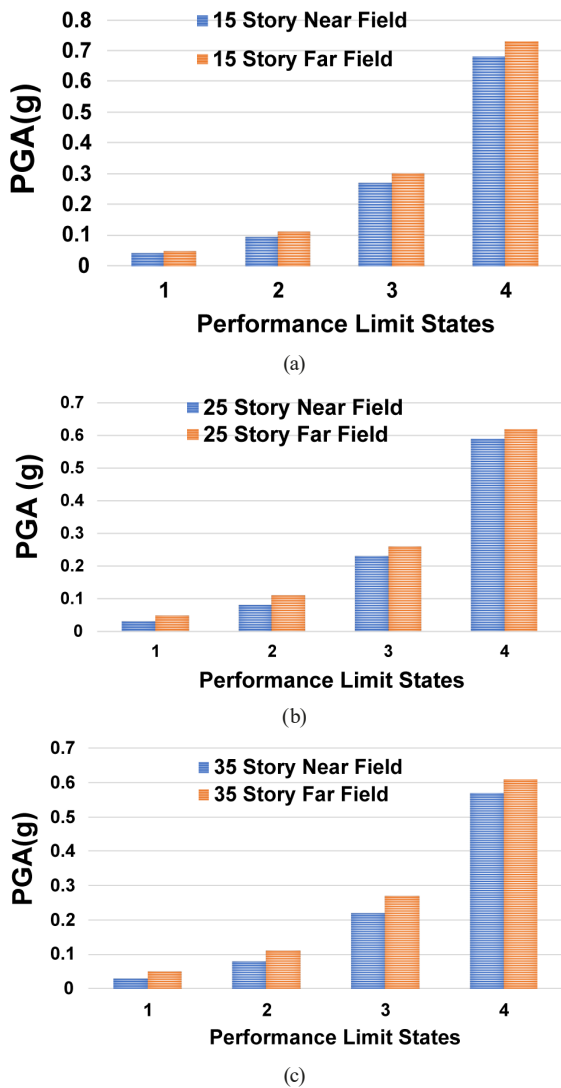


Fig. 25 Median fragility for all research models; (a) 15 Story Models, (b) 25 Story Models, (c) 35 Story Models

Analyzing different types of RC SMRFs equipped with BRBs confirmed that height increase influences the slight and moderate damage levels but is more pronounced in structures in extensive and complete collapse levels. Given that the slight and moderate damage levels are reached within elastic limit, the difference of 40% in the median fragility of these two levels is not as noticeable as the 6%

difference between near-field and far-field earthquakes for the extensive and complete collapse levels, which are corresponding to the nonlinear performance of structures. Considering the curves plotted and the median fragility results obtained, the near-fault high-rise structures are more vulnerable and reach the four damage levels earlier. This point has been addressed in the guidelines for damage threshold drifts of high-rise structures. Table 10 summarizes the difference in vulnerability increase of near-field and far-field structures.

Table 10 shows that vulnerability has increased in all damage levels for the entire near-field models compared to their far-field companions. Besides, seismic fragility increases with increasing height in the elastic region corresponding to slight damage level. However, vulnerability of higher structures decreases in moderate damage level. As more damage is sustained up to reaching the complete collapse of structures, variations in vulnerability increase, as a consequence of distance from fault, coincide for all models, accounting for the difference in height and number of stories.

Considering Fig. 26, vulnerability variations against height of structures are quite evident. In this regard, the higher the level of damage, the less noticeable the change. In terms of considering drift, however, even slight changes are of significance.

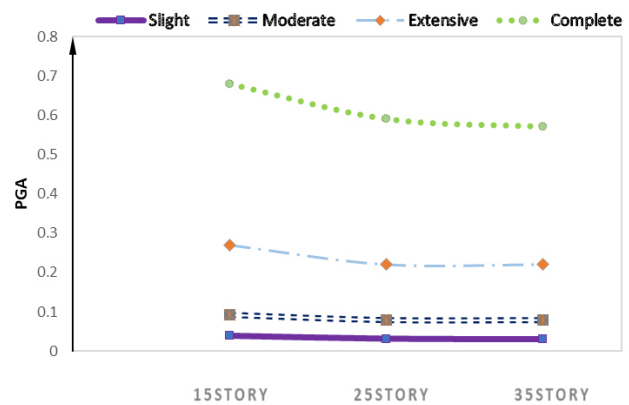


Fig. 26 Comparison of near-field median fragility in four limit states

Table 10 Difference in vulnerability increase of near-fault structures

Model	Slight Limit State Fragility Difference	Moderate Limit State Fragility Difference	Extensive Limit State Fragility Difference	Complete Damage Limit State Fragility Difference
15-Story Near Field	19	19	10	7
25-Story Near Field	39	29	23	5
35-Story Near Field	40	17	18	6

References

- [1] Kennedy, R. P., Cornell, C. A., Campbell, R. D., Kaplan, S., Perla, H. F. "Probabilistic seismic safety study of an existing nuclear power plant ", *Nuclear Engineering and Design*, 59(2), pp. 315–338, 1980.
[https://doi.org/10.1016/0029-5493\(80\)90203-4](https://doi.org/10.1016/0029-5493(80)90203-4)
- [2] Alavi, B., Krawinkler, H. "Effects of near-fault ground motions on frame structures", *The John A. Blume Earthquake Engineering Center, California, USA, Rep. 138*, 2001.
- [3] Somerville, P. G. "Magnitude scaling of the near fault rupture directivity pulse", *Physics of the Earth and Planetary Interiors*, 137(1–4), pp. 201–212, 2003.
[https://doi.org/10.1016/S0031-9201\(03\)00015-3](https://doi.org/10.1016/S0031-9201(03)00015-3)
- [4] Vafaei, D., Eskandari, R. "Seismic response of mega buckling-restrained braces subjected to fling-step and forward-directivity near-fault ground motions", *Tall and Special Buildings*, 24(9), pp. 672–686, 2014.
<https://doi.org/10.1002/tal.1205>
- [5] Wakabayashi, M., Nakamura, T., Kashibara, A., Morizono, T., Yakoyama, H. "Experimental study of elastoplastic properties of precast concrete wall panels with built-in insulating braces", *Summaries of Technical Papers of Annual Meeting, Architectural Institute of Japan*, pp. 1041–1044, 1973.
- [6] Uang, C. M., Nakashima, M., Tsai, K. C. "Research and application of buckling-restrained braced frames", *Steel Structures*, 4(1), pp. 301–313, 2004.
- [7] Uriz, P. "Towards Earthquake Resistant Design of Concentrically Braced Steel Structures", PhD Thesis, University of California, 2005.
- [8] Lin, K.-C., Lin, C.-C. J., Chen, J.-Y., Chang, H.-Y. "Seismic reliability of steel framed buildings", *Structural Safety*, 32(3), pp. 174–182, 2010.
<https://doi.org/10.1016/j.strusafe.2009.11.001>
- [9] Krishnan, S., Ji, C., Komatitsch, D., Tromp, J. "Performance of Two 18-Story Steel Moment-Frame Buildings in Southern California During Two Large Simulated San Andreas Earthquakes", *Earthquake Spectra*, 22(4), pp. 1035–1061, 2010.
<https://doi.org/10.1193%2F1.2360698>
- [10] Huang, S. N., Lu, X. Z., Ye, L. P. "Study on the Strengthening Effect of a Typical RC Frame in Wenchuan Earthquake with Attached Substructures", *Applied Mechanics and Materials*, 353–356, pp. 2057–2064, 2013.
<https://doi.org/10.4028/www.scientific.net/AMM.353-356.2057>
- [11] Shin, J., Kim, J., Lee, K. "Fragility Assessment of Damaged Piloti-Type RC Building With/Without BRB Under Successive Earthquakes", *Journal of the Earthquake Engineering Society of Korea*, 17(3), pp. 133–141, 2013.
<https://doi.org/10.5000/EESK.2013.17.3.133>
- [12] Merczel, D. B., Somja, H., Aribert, J.-M., Lógó, J. "On the behaviour of concentrically braced frames subjected to seismic loading", *Periodica Polytechnica Civil Engineering*, 57(2), pp. 113–122, 2013.
<https://doi.org/10.3311/PPci.7167>
- [13] Khampanit, A., Leelataviwat, S., Kochanin, J., Warnitchai, P. "Energy-based seismic strengthening of non-ductile reinforced concrete frames using buckling-restrained braces", *Engineering Structures*, 81(1), pp. 110–122, 2014.
<https://doi.org/10.1016/j.engstruct.2014.09.033>
- [14] Della Corte, G., D'Aniello, M., Landolfo, R. "Field-Testing of All Buckling restrained Braces Applied to a Damage Reinforced Concrete Building", *Journal of Structural Engineering*, 141(1), pp. 1943–1954, 2015.
[https://doi.org/10.1061/\(ASCE\)ST.1943-541X.0001080](https://doi.org/10.1061/(ASCE)ST.1943-541X.0001080)
- [15] Merczel, D. B., Aribert, J.-M., Somja, H., Hjjaj, M. "Plastic analysis-based seismic design method to control the weak storey behaviour of concentrically braced steel frames", *Journal of Constructional Steel Research*, 125(1), pp. 142–163, 2016.
<https://doi.org/10.1016/j.jcsr.2016.05.008>
- [16] Pan, K.-Y., Wu, A.-C., Tsai, K.-C., Li, C.-H., Khoo, H.-H. "Seismic retrofit of reinforced concrete frames using buckling-restrained braces with bearing block load transfer mechanism", *Earthquake Engineering Structural Dynamics*, 45(14), pp. 2303–2326, 2016.
<https://doi.org/10.1002/eqe.2763>
- [17] Khoo, H.-H., Tsai, K.-C., Tsai, C.-Y., Wang, K.-J. "Bidirectional substructure pseudo-dynamic tests and analysis of a full-scale two-story buckling-restrained braced frame", *Earthquake Engineering and Structural Dynamics*, 45(7), pp. 1087–1107, 2016.
<https://doi.org/10.1002/eqe.2696>
- [18] Hamidi Jamnani, H., Abdollahzadeh, G., Faghimaleki, H. "Seismic fragility analysis of improved RC frames using different type of bracing", *Journal of Engineering Science and Technology*, 12(4), pp. 913–934, 2017.
- [19] Zsarnóczay, A., Balogh, T., Vigh, L. G. "On the European Norms of Design of Buckling Restrained Braced Frames", *The Open Civil Engineering Journal*, 11(Sup.1-M16), pp. 513–530, 2017.
<https://doi.org/10.2174/1874149501711010513>
- [20] Freddi, F., Padgett, J. E., Dall'asta, A. "Life Cycle Cost Analysis of Low Ductility RC Frame Buildings Retrofitted by Modern Retrofit Techniques", In: *EACS 5th European Conference on Structural Control*, Genoa, Italy, 2012, Paper No. 92 (pp. 1–8). ISBN: 9788895023137
<https://discovery.ucl.ac.uk/id/eprint/1575832>
- [21] Almeida, A., Ferreira, R., Proença, J. M., Gago, A. S. "Seismic retrofit of RC building structures with Buckling Restrained Braces", *Engineering Structures*, 130(1), pp. 14–22, 2017.
<https://doi.org/10.1016/j.engstruct.2016.09.036>
- [22] Gong, J., Zhu, Z., Zeng, C. "Review of Research and Application of Reinforced Concrete Structures Strengthened by Braces", In: *The 2nd International Conference on Civil Engineering and Materials Science*, Seoul, Korea, 2017, 012025.
<https://doi.org/10.1088/1757-899X/216/1/012025>
- [23] Tsai, C.-Y., Tsai, K.-C., Chen, L.-W., Wu, A. C. "Seismic performance analysis of BRBs and gussets in a full-scale 2-story BRB-RCF specimen", *Earthquake Engineering and Structural Dynamics*, 47(12), pp. 2366–2389, 2018.
<https://doi.org/10.1002/eqe.3073>

- [24] Del Gobbo, G. M., Williams, M. S., Blakeborough, A. "Seismic performance assessment of Eurocode 8-compliant concentric braced frame buildings using FEMA P-58", *Engineering Structures*, 155(1), pp. 192–208, 2018.
<https://doi.org/10.1016/j.engstruct.2017.11.016>
- [25] Qie, Y., Barbagallo, F., Marino, E. M., Du, C., Wang, T. "Full-scale hybrid test for realistic verification of a seismic upgrading technique of RC frames by BRBs", *Earthquake Engineering and Structural Dynamics*, 49(14), pp. 1452–1472, 2020.
<https://doi.org/10.1002/eqe.3312>
- [26] Pahlavan, H., Zarif Moghadam Basefat, A., Shamekhi Amiri, M., Namirani, P. "Probabilistic Seismic Performance assessment of tall buildings having special RC moment frames equipped with buckling restrained braces (BRB)", *Journal of Structural and Construction Engineering*, 4(4), 58–78, 2018. (in Persian)
<https://doi.org/10.22065/jsce.2020.198620.1929>
- [27] Bai, J., Chen, H., Jin, S. "Investigation on the interaction between BRBs and the RC frame in BRB-RCF systems", *Engineering Structures*, 243(3), 112685, 2021.
<https://doi.org/10.1016/j.engstruct.2021.112685>
- [28] Chen, H., Bai, J. "Seismic performance evaluation of buckling-restrained braced RC frames considering stiffness and strength requirements and low-cycle fatigue behaviors", *Engineering Structures*, 239(2), 112359, 2021.
<https://doi.org/10.1016/j.engstruct.2021.112359>
- [29] Department of Homeland Security Federal Emergency Management Agency "HAZUS -MH MR5", *Advanced Engineering Building Module*, Washington, DC, USA, 2003.
- [30] BHRC "Iranian National Building Regulations", (6th Ed.), Road, Housing and Urban Development Research Center, Tehran, Iran, 2013.
- [31] Iranian Building Codes and Standards "Iranian Code of Practice for Seismic Resistant Design of Buildings", (4th Ed.), Road, Housing and Urban Development Research Center, Tehran, Iran, 2014.
- [32] Chopra, A. K., Chintanapakdee, C. "Inelastic Deformation Ratios for Design and Evaluation of Structures: Single-Degree-of-Freedom Bilinear Systems", *Journal of Structural Engineering*, 130(9), Rep. EERC 2003-09, 2004.
[https://doi.org/10.1061/\(ASCE\)0733-9445\(2004\)130:9\(1309\)](https://doi.org/10.1061/(ASCE)0733-9445(2004)130:9(1309))
- [33] Applied Technology Council "Earthquake Damage Evaluation Data for California", *Federal Emergency Management Agency*, Redwood, CA, USA, Rep. CA 94065, 1985.
- [34] American Society of Civil Engineering "Minimum Design Loads and Associated Criteria for Buildings and Other Structures (ASCE/SEI 7-22)", *Structural Engineering Institute (SEI)*, Reston, VA, USA, 2022.
- [35] Uang, C.-M. "Establishing R (or R_w) and C_d Factors for Building Seismic Provisions", *Journal of Structural Engineering*, 117(1), pp. 19–28, 1991.
[https://doi.org/10.1061/\(ASCE\)0733-9445\(1991\)117:1\(19\)](https://doi.org/10.1061/(ASCE)0733-9445(1991)117:1(19))
- [36] Elnashai, A. S. "Do We Really Need Inelastic Dynamic Analysis?", *Journal of Earthquake Engineering*, 6(1), pp. 123–130, 2009.
<https://doi.org/10.1080/13632460209350435>
- [37] Mander, J. B., Priestley, M. J. N., Park, R. "Theoretical stress-strain model for confined concrete", *Journal of Structural Engineering*, 114(8), pp. 1804–1826, 1988.
[https://doi.org/10.1061/\(ASCE\)0733-9445\(1988\)114:8\(1804\)](https://doi.org/10.1061/(ASCE)0733-9445(1988)114:8(1804))
- [38] Applied Technology Council "Quantification of building seismic performance factor", *Federal Emergency Management Agency*, Redwood, CA, USA, Rep. CA 94065, 2009.
- [39] Shome, N. "Probabilistic seismic demand analysis of nonlinear structures", *PhD Thesis*, Stanford University, 1999.
- [40] Lu, X., Liao, W., Cui, Y., Jiang Q., Zhu, Y. "Development of a novel sacrificial-energy dissipation outrigger system for tall buildings", *Earthquake Engineering and Structural Dynamics*, 48(15), pp. 1661–1677, 2019.
<https://doi.org/10.1002/eqe.3218>